Many-body calculations and hyperfine-interaction effect on dynamic polarizabilities at the low-lying energy levels of Y^{2+}

Arghya Das,[1,*] Anal Bhowmik,[2,3,†] Narendra Nath Dutta,[4] and Sonjoy Majumder[1,‡]

[1]*Department of Physics, Indian Institute of Technology Kharagpur, Kharagpur 721302, India*
[2]*Haifa Research Center for Theoretical Physics and Astrophysics, University of Haifa, Haifa 3498838, Israel*
[3]*Department of Mathematics, University of Haifa, Haifa 3498838, Israel*
[4]*Department of Chemical Sciences, Indian Institute of Science Education and Research Mohali, Punjab 140306, India*

The present paper determines the precise values of magic wavelengths corresponding to the clock transitions 5^2S–4^2D of the Y^{2+} ion at the levels of both fine and hyperfine structures due to the external light beams having linear as well as circular polarization. To calculate the dynamic polarizabilities of the associated states of the transitions, we employ the sum-over-states technique, where the dominating and correlation sensitive part of the sum is evaluated using a highly correlated relativistic coupled-cluster theory. The estimated magic wavelengths of the light beams have substantial importance to cool and trap the ion using a blue-detuned trapping scheme. We also present the tune-out wavelengths, which are useful in state-insensitive trapping and cooling. The vector component of a total polarizability, which is induced by a circularly polarized light only, can provide additional magic wavelengths. Considerable effects of hyperfine interaction on the values of polarizabilities and number of magic wavelengths divulge the importance of precise estimations of hyperfine-structure splitting.

I. INTRODUCTION

Accurate information about the dynamic polarizabilities of the atomic states at the hyperfine levels can be significant for quantum experiments such as trapping and cooling [1–3], atom interferometry [4,5], quantum registers [6], etc.. Also, appropriate environments for cooling and trapping of ions are absolutely necessary to perform error-free experiments for frequency standard [7], fundamental constants [8–10], quantum computers [11], and many other modern advanced technologies [12–15]. For instance, the preciseness of trapping and cooling parameters of ions mostly decides the fractional uncertainties of frequency standards, which are sought to be of the order of 10^{-18} or less than this [16–18]. It has been shown over the past two decades that singly [19], doubly [20,21], or multiply [8] charged ions can be competing candidates for the frequency standard in terms of accuracy and stability. Since the perturbation due to the external field reduces with increasing ionization for an atomic system [22], doubly ionized systems can be better choices than singly ionized atoms for many of the above-mentioned experiments. Besides the increasing ionicity, the other way to improve the accuracy is to prepare the states and transitions among them insensitive to external field [21,23–29].

The narrow linewidth quadrupole transitions between ground states and long-lived metastable states of some moderate to heavy ions are being targeted from a long past for quantum experiments, such as atomic clocks [30–34],

quantum computers [35], etc.. Rubidium-like Sr^+, which has the ground state $5^2S_{\frac{1}{2}}$, is a well-known ion for quantum technology and $5^2S_{\frac{1}{2}}$–$4^2D_{\frac{3}{2},\frac{5}{2}}$ quadrupole transitions of this ion are particularly utilized in quantum computing [36,37]. Here we are proposing the same narrow linewidth transition of Y^{2+}, but now the ground state is $4^2D_{\frac{3}{2}}$ instead of $5^2S_{\frac{1}{2}}$. However, as indicated earlier, the advantage of using Y^{2+} instead of Sr^+ is that the atomic states of Y^{2+} are affected less by the perturbation of the electric field of the laser beam due to one unit more positive charge. But, certainly, the effect of this perturbation cannot be avoided for Y^{2+} in general experimental circumstances. Nevertheless, with the advent of cryogenic methods, highly charged ions are also possible to keep cool for a longer period [38], and, therefore, Y^{2+} can be extremely important for trap-assisted experimental studies.

Further, a recent experiment on the isotope shift of the $5^2S_{\frac{1}{2}} \rightarrow 5^2P_{\frac{1}{2}}$ transition of the Y^{2+} ion at 294.6 nm [39], where optical pumping ($4^2D_{\frac{3}{2}} \rightarrow 5^2P_{\frac{3}{2}}$) is achieved by a 232.7-nm laser source, motivates us to propose the $4^2D_{\frac{3}{2}} \rightarrow 5^2S_{\frac{1}{2}}$ transition (clock transition) for the above-mentioned quantum experiments. This is evident from the energy-level diagram in Fig. 1 indicating possible cooling and clock transitions of Y^{2+} among the level positions of all the five states. These prodigious technological and conceptual advancements on quantum experiments cannot be worthwhile for precision measurements without the proper choice of wavelengths of the external field at which the differential ac Stark shift between the associated energy levels of the atom or ion vanishes. The corresponding wavelengths are called magic wavelengths [40]. In addition, the precise measurements of the tune-out

———————
*arghyadas@iitkgp.ac.in
†abhowmik@campus.haifa.ac.il
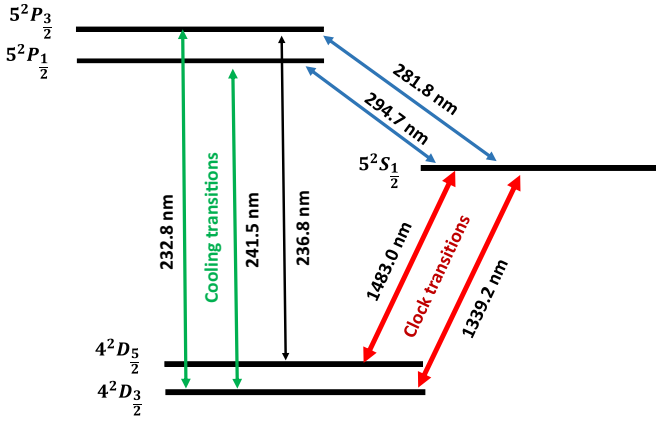‡sonjoym@phy.iitkgp.ernet.in

FIG. 1. The clock (indicated by red color) and cooling (indicated by green color) transitions of Y^{2+}.

wavelengths of light, where the polarizability of an atomic state vanishes, are crucial for atom interferometry [41].

Whereas a linearly polarized beam can induce scalar and tensor components of a valence polarizability, the circularly polarized light can add a vector component to that. This vector part of the polarizability arises from the induced dipole moment perpendicular to the polarization of the field. As a consequence, use of a circularly polarized light is advantageous in many situations of the quantum experiments [7]. The urge to find these magic and tune-out wavelengths inspires theorists for highly accurate calculations on the dynamic polarizabilities of the electronic states of atoms or ions involved in the experiments. Here we are interested in evaluating dynamic polarizabilities of the ground ($4^2D_{\frac{3}{2}}$), first-excited ($4^2D_{\frac{5}{2}}$), and second-excited ($5^2S_{\frac{1}{2}}$) states of Y^{2+}. Another advantage of using Y^{2+} is the relatively long lifetime of the first (244.08 s) and second (10.76 s) excited states [42] of this ion. In addition to these three clock states, the $5^2P_{\frac{1}{2},\frac{3}{2}}$ states of Y^{2+} are also important for the cooling transitions $4^2D_{\frac{3}{2},\frac{5}{2}} \rightarrow 5^2P_{\frac{1}{2},\frac{3}{2}}$ achievable at 230–245 nm [39,43–48]. Therefore, the precise knowledge of static and dynamic polarizabilities of these five low-lying states of Y^{2+} is important in conducting trap-assisted precision experiments on this ion. Moreover, it is important to note that the scalar component of the static polarizability provides the theoretical estimation of the blackbody radiation shift [40,49–51], one of the important inputs to determine the clock accuracy.

Precise knowledge of hyperfine-structure constants or hyperfine constants of atoms and ions can be an important requirement in many experiments associated with the dynamic polarizabilities of hyperfine multiplets of the clock states. Experiments on the hyperfine splittings are also known as one of the first applications of trapped ions [52,53]. Moreover, the hyperfine constants are also important in an investigation of chemical composition of the Sun and stars. Being one of the astrophysically important elements [54–56], hyperfine constants of Y^{2+} thus need a highly accurate theoretical treatment. So far, there has been one recent work [39] along with a very old experiment [57] providing hyperfine constants only for $5^2S_{\frac{1}{2}}$ and $5^2P_{\frac{1}{2}}$ states of Y^{2+}. However, such values

are also needed to be estimated for the other states as well theoretically and/or experimentally.

We further calculate the dynamic polarizabilities of the $4^2D_{\frac{3}{2},\frac{5}{2}}$ and $5^2S_{\frac{1}{2}}$ states at the hyperfine levels and estimate the magic wavelengths for the $5^2S_{\frac{1}{2}}$–$4^2D_{\frac{3}{2}}$ and $5^2S_{\frac{1}{2}}$–$4^2D_{\frac{5}{2}}$ clock transitions in the presence of a linearly and a circularly polarized light. For a particular hyperfine multiplet, the tune-out wavelength due to a circularly polarized light shifts with respect to the tune-out wavelength due to a linearly polarized light and this shift is a measure of fictitious magnetic field useful for trapping and cooling [58]. To calculate the dynamic polarizabilities of the clock states at both the fine- and hyperfine-structure levels and the static polarizabilities of the $5^2P_{\frac{1}{2},\frac{3}{2}}$ states, we have employed a highly accurate relativistic many-body formalism. The details of this formalism are discussed at the end of Sec. II and the beginning of Sec. III.

II. THEORY

The Stark shift ($\Delta\xi_v$) for a single-valence atom or ion with the valence electron in the vth orbital is obtained by the second-order time-independent perturbation theory [40]

$$\Delta\xi_v(\omega) = \sum_{i \neq v} \frac{1}{\omega_{vi}} |\langle\psi_v| - \mathbf{D} \cdot \mathbf{E}|\psi_i\rangle|^2 = -\frac{1}{2}\alpha_v(\omega)E^2 \quad (1)$$

where E is the strength of the applied electric field at the position of the atom, $-\mathbf{D} \cdot \mathbf{E}$ is the electric dipole interaction Hamiltonian, and $\omega_{vi} = \epsilon_v - \epsilon_i$ is the resonance frequency associated with the electric dipole ($E1$) transition between the states $|\psi_v\rangle$ and $|\psi_i\rangle$. Due to the frequency dependence of $\mathbf{E}$, i.e., $\mathbf{E}(\omega)$, the electric dipole polarizability α_v of the state $|\psi_v\rangle$ also becomes frequency dependent, $\alpha_v(\omega)$, and can be decomposed into three components [21,40]:

$$\alpha_v(\omega) = \alpha_v^C(\omega) + \alpha_v^{VC}(\omega) + \alpha_v^V(\omega). \quad (2)$$

$\alpha_v^C(\omega)$ represents the contribution to the total polarizability due to the ionic core [21,40], and its value is irrespective of the presence of the valence electron at any orbital. It can be expressed as [21,40,59]

$$\alpha_v^C(\omega) = \frac{2}{3} \sum_{ap} \frac{|\langle\phi_a||d_{\mathrm{DF}}||\phi_p\rangle\langle\phi_a||d_{\mathrm{RMBPT(2)}}||\phi_p\rangle|\omega_{pa}}{(\omega_{pa})^2 - \omega^2}. \quad (3)$$

The subscripts a and p in Eq. (3) indicate the core (fully occupied) and virtual (fully unoccupied) orbitals, respectively, with respect to the electron distributions for the ionic core. $\langle\phi_a||d_{\mathrm{DF}}||\phi_p\rangle$ and $\langle\phi_a||d_{\mathrm{RMBPT(2)}}||\phi_p\rangle$ represent the reduced electric dipole matrix elements obtained from the Dirac-Fock (DF) method [60,61] and the second-order relativistic manybody perturbation theory [RMBPT(2)] [59], respectively. In one of the works regarding Eq. (3), Mitroy *et al.* [40] mentioned an all-order theory like the random-phase approximation (RPA) [59] method with respect to our RMBPT(2) method. The conversion formula from a RPA matrix element to a corresponding RMBPT(2) matrix element is discussed in the work of Johnson *et al.* [59] using diagrammatic perturbation theory. Nevertheless, for alkali-metal-like systems, the RMBPT(2) can provide a good approximation to the RPA in

the calculation of core polarizability and this is tested by us for a number of such systems. $\alpha_v^{VC}(\omega)$ is the perturbation to the core polarizability in the presence of the valence electron [21,62]. This component of the polarizability is almost frequency independent within the frequency range considered in this paper.

The estimation of $\alpha_v^V(\omega)$ is the most crucial part for the calculation of the total dynamic polarizability and can be performed by using the following relationship [63]:

$$\alpha_v^V(\omega) = \alpha_v^{(0)}(\omega) + \sigma \frac{M_{J_v}}{2J_v}\alpha_v^{(1)}(\omega)$$
$$+ \frac{3M_{J_v}^2 - J_v(J_v+1)}{J_v(2J_v-1)}\alpha_v^{(2)}(\omega). \quad (4)$$

Here J_v and M_{J_v} are the total angular momentum and its projection component for the state $|\psi_v\rangle$, respectively. The polarization factor σ is zero for a linearly polarized light and ± 1 for a circularly polarized light. This implies that the vector component of the valence polarizability is the only factor to differentiate between the impact caused by a linearly polarized light and the impact caused by a circularly polarized light. $\alpha_v^{(0)}(\omega)$, $\alpha_v^{(1)}(\omega)$, and $\alpha_v^{(2)}(\omega)$ are the three components of the total valence polarizability specifying scalar, vector, and tensor parts, respectively. Here, by "scalar," we only mean the scalar part of the valence polarizability, unless otherwise indicated. In the sum-over-states formalism, these components are expressed as [21,29,63]

$$\alpha_v^{(0)}(\omega) = \frac{2}{3(2J_v+1)}\sum_n d_{nv}, \quad (5)$$

$$\alpha_v^{(1)}(\omega) = -\sqrt{\frac{6J_v}{(J_v+1)(2J_v+1)}}\sum_n (-1)^{J_n+J_v}$$
$$\times \begin{Bmatrix} J_v & 1 & J_v \\ 1 & J_n & 1 \end{Bmatrix}\left(\frac{2\omega}{\omega_{nv}}\right)d_{nv}, \quad (6)$$

and

$$\alpha_v^{(2)}(\omega) = 4\sqrt{\frac{5J_v(2J_v-1)}{6(J_v+1)(2J_v+1)(2J_v+3)}}\sum_n (-1)^{J_n+J_v}$$
$$\times \begin{Bmatrix} J_v & 1 & J_n \\ 1 & J_v & 2 \end{Bmatrix}d_{nv}, \quad (7)$$

where the apparently angular momentum independent factor $d_{nv} = \{|\langle\psi_v||d||\psi_n\rangle|^2\omega_{nv}\}/(\omega_{nv}^2-\omega^2)$ diverges at resonant frequency $\omega_{nv} = \epsilon_n - \epsilon_v$.

At a hyperfine energy level F_v with nuclear spin I, the valence polarizability $[\alpha_{vF}^V(\omega)]$ can be written in a similar mathematical form as of Eq. (4), but with replacement of total angular momentum and its projection quantum number (J_v, M_{J_v}) by the corresponding hyperfine and its projection quantum number (F_v, M_{F_v}) with $\mathbf{F}_v = \mathbf{J}_v + \mathbf{I}$. Also, the expression for the hyperfine-induced scalar part of the valence polarizability, $\alpha_{vF}^{(0)}(\omega)$, is equal to $\alpha_v^{(0)}(\omega)$ as the second-order scalar shift does not depend on any hyperfine quantum number [64]. However, the hyperfine-induced vector and tensor parts, $\alpha_{vF}^{(1)}(\omega)$ and $\alpha_{vF}^{(2)}(\omega)$, respectively, have extra factors following angular momentum algebra. These polarizabilities are related to the corresponding hyperfine-independent polarizabilities

$\alpha_v^{(1)}(\omega)$ and $\alpha_v^{(2)}(\omega)$, respectively, by the following expressions [64–66]:

$$\alpha_{vF}^{(1)}(\omega) = (-1)^{J_v+F_v+I+1}\begin{Bmatrix} F_v & J_v & I \\ J_v & F_v & 1 \end{Bmatrix}$$
$$\times \sqrt{\frac{F_v(2F_v+1)(2J_v+1)(J_v+1)}{J_v(F_v+1)}}\alpha_v^{(1)}(\omega) \quad (8)$$

and

$$\alpha_{vF}^{(2)}(\omega) = (-1)^{J_v+F_v+I}\begin{Bmatrix} F_v & J_v & I \\ J_v & F_v & 2 \end{Bmatrix}$$
$$\times \sqrt{\left(\frac{F_v(2F_v-1)(2F_v+1)}{(2F_v+3)(F_v+1)}\right)}$$
$$\times \sqrt{\left(\frac{(2J_v+3)(2J_v+1)(J_v+1)}{J_v(2J_v-1)}\right)}\alpha_v^{(2)}(\omega). \quad (9)$$

The hyperfine shift (HFS) and splitting in the energy can be calculated accurately from the precise knowledge of hyperfine-structure constants corresponding to the magnetic dipole and electric quadrupole moments of the nucleus, which are known as the hyperfine A and B constants, respectively [67,68]. The definitions of the above constants in terms of reduced matrix elements of the Hamiltonians corresponding to these nuclear moment interactions to the electronic sector are as follows [68,69]:

$$A = \mu_N g_I \frac{\langle J_v||\mathbf{T}^{(1)}||J_v\rangle}{\sqrt{J_v(J_v+1)(2J_v+1)}} \quad (10)$$

and

$$B = 2eQ\sqrt{\frac{2J_v(2J_v-1)}{(2J_v+1)(2J_v+2)(2J_v+3)}}\langle J_v||\mathbf{T}^{(2)}||J_v\rangle, \quad (11)$$

where μ_N is the nuclear magneton, g_I is the nuclear g factor, and Q is the quadrupole moment of the nucleus. The operators $\mathbf{T}^{(1)}$ and $\mathbf{T}^{(2)}$ can be written in terms of the spherical harmonic operators Y_{kq} and the Dirac matrix $\boldsymbol{\alpha}$ using the following relations [68]:

$$\mathbf{T}_q^{(1)} = \sum_j \mathbf{t}_q^{(1)} = \sum_j -ie\sqrt{8\pi/3}r_j^{-2}\boldsymbol{\alpha}_j.\mathbf{Y}_{kq}(\hat{r}_j), \quad (12)$$

$$\mathbf{T}_q^{(2)} = \sum_j \mathbf{t}_q^{(2)} = \sum_j -er_j^{-3}\sqrt{\frac{4\pi}{2k+1}}\mathbf{Y}_{kq}(\hat{r}_j) \quad (13)$$

with $k = 1$ and 2 for $\mathbf{T}^{(1)}$ and $\mathbf{T}^{(2)}$, respectively. The sum over j implies the sum over all the electronic coordinates [68]. With the computed values of A and B constants, the HFS of an atomic energy level can be calculated almost precisely (the higher-order nuclear moments like the nuclear octupole moment can contribute to HFS with very little impact) using the formula [68]

$$E_{\text{HFS}} = \frac{AK}{2} + \frac{1}{2}\frac{3K(K+1) - 4J_v(J_v+1)I(I+1)}{2I(2I-1)2J_v(2J_v-1)}B, \quad (14)$$

where $K = F_v(F_v+1) - I(I+1) - J_v(J_v+1)$.

The parameters which require exhaustive many-body treatment in the computations of the polarizabilities and hyperfine

constants are the associated reduced matrix elements and the energy eigenvalues. In this paper, we use three different theoretical approaches: DF, RMBPT(2), and relativistic coupled-cluster method with single, double, and partial triple excitations [RCCSD(T)] [70,71], in a case-by-case basis with a compromise between accuracy and computational effort. This is elaborated in the next section. Nevertheless, very brief but adequate descriptions of the DF and RMBPT(2) theories are available in the work of Reiher and Hess [72] and Johnson *et al.* [59]. The details of the DF theory with an algorithm of its computational implementation are given in [60,61], whereas the RMBPT(2) theory is discussed in [73,74]. The RCCSD(T) is a well-known many-body method for the calculations of electronic-structure properties accurately from a long time [73–81]. The RCCSD(T) method is discussed in detail in a review article of Bartlett and Musial [80]; brief discussions on the different correlation mechanisms corresponding to the different levels of cluster excitations and their numerical contributions can be found in our earlier works [76,81–84].

III. RESULTS AND DISCUSSIONS

A. Dynamic polarizabilities and magic wavelengths for fine-structure states

We use sum-over-states formalism, as explained in the last section, to estimate the dynamic polarizabilities of $4^2D_{\frac{3}{2}, \frac{5}{2}}$ and $5^2S_{\frac{1}{2}}$ states along with the static polarizabilities of these three states and $5^2P_{\frac{1}{2}, \frac{3}{2}}$ states. According to this formalism [see Eqs. (5)–(7)], the accurate calculations of a large number of $E1$ matrix elements can be seen as essential for the accurate calculations of the scalar, vector, and tensor parts of the total valence polarizability. The summation index (n) in Eqs. (5)–(7) refers to the different intermediate single-valence open-shell states $|\psi_n\rangle$. These states correspond to different principal and angular momentum quantum numbers of the valence orbitals. The angular momentum quantum numbers are selected such that $\langle\psi_v||d||\psi_n\rangle \neq 0$ according to the $E1$ selection rule. In the present calculations, the principal quantum number is considered up to 25, beyond which the $E1$ matrix elements have very negligible contributions to the total valence polarizabilities.

As mentioned in the last paragraph of the previous section, depending on the comparative strengths of the $E1$ matrix elements in evaluating the valence polarizabilities, we consider three different levels of many-body theories: RCCSD(T), RMBPT(2), and DF. However, the former two correlated many-body theories are also based on the generations of DF orbitals to construct the zeroth-order wave functions. Nonetheless, these DF orbitals are constructed using Gaussian-type-orbital (GTO) basis functions [61,76] of the type $r^{n_\kappa}e^{-\alpha_i r^2}$ with $\alpha_i = \alpha_0\beta^{i-1}$, where α_0 and β are considered as 0.00525 and 2.73, respectively. The values of i are 1, 2, 3, . . . , N, where N is the size of the basis set [61] for each symmetry. n_κ is a constant the values of which are 1, 2, 3, 4, 5, and 6 for s, p, d, f, g, and h symmetries, respectively. [61]. The sizes of the basis set considered for the above-mentioned symmetries are 33, 30, 28, 25, 21, and 20, respectively [42]. The RCCSD(T) and RMBPT(2) calculations also require adequate inclusions of active-orbital basis

sets to satisfy the correlation energy convergence criteria [76], which are considered as 11, 11, 13, 11, 10, and 6 in numbers for the s, p, d, f, g, and h symmetries, respectively.

In the sum-over-states strategy, the most dominant contribution to a valence polarizability appears from the sum [Eqs. (5)–(7)] of the terms having $E1$ matrix elements associated with the first few low-lying states. Accordingly, the excited states $5–8^2S_{\frac{1}{2}}$, $5–8^2P_{\frac{1}{2}, \frac{3}{2}}$, $4–7^2D_{\frac{3}{2}, \frac{5}{2}}$, and $4–6^2F_{\frac{5}{2}, \frac{7}{2}}$ are found to be the most important states in the present sum-over-states formalism. The matrix elements are calculated here using the correlation exhaustive RCCSD(T) method, and the corresponding transition energies to calculate valence polarizability are extracted from the website of the National Institute of Standards and Technology [85]. Relatively less important $E1$-matrix elements of the sum are calculated by using RMBPT(2) [59], which includes core polarization corrections on top of the DF contributions [73,86]. This part sums up the contributions from the next five single valence states for all the symmetries. The $E1$ matrix elements, the contributions of which have little significance to the total valence polarizabilities, are associated with the single valence states $14–25^2S_{\frac{1}{2}}$, $14–25^2P_{\frac{1}{2}, \frac{3}{2}}$, $13–25^2D_{\frac{3}{2}, \frac{5}{2}}$, and $12–25^2F_{\frac{5}{2}, \frac{7}{2}}$. The wave functions and the corresponding $E1$ matrix elements of these states are calculated using the DF method only.

In Table I, we represent total static polarizabilities [$\alpha_v(0)$] of $4^2D_{\frac{3}{2}, \frac{5}{2}}$, $5^2S_{\frac{1}{2}}$, and $5^2P_{\frac{1}{2}, \frac{3}{2}}$ states for the case $J_v = M_{J_v}$. The contributions from $\alpha_v^C(0)$ and $\alpha_v^{VC}(0)$ to the total static polarizabilities are also presented along with the scalar [$\alpha_v^{(0)}(0)$] and tensor [$\alpha_v^{(2)}(0)$] components of $\alpha_v^V(0)$. The decomposition of $\alpha_v^V(0)$ in terms of the RCCSD(T), RMBPT(2), and DF parts as discussed in the previous paragraph of this section is shown quantitatively in Table II. Nevertheless, our calculated values of the polarizabilities for the clock states in Table I are compared with the corresponding theoretical values of Safronova and Safronova [87]. They used an all-order relativistic many-body perturbation theory, which is very similar to a linearized coupled-cluster theory, for their calculation for the valence part of a polarizability. Our RCCSD(T) method, which is employed to calculate the most dominating part of a valence polarizability, is theoretically more accurate than their all-order method as the former is augmented with important nonlinear terms. However, their method corresponds to use of the RPA matrix element with respect to our RMBPT(2) matrix element to compute the core polarizability [40,87,88]. As mentioned in the previous section, our calculated value of core polarizability 4.28 a.u. is an approximation to the all-order RPA value of core polarizability 4.05 a.u. Here it should be mentioned that indeed our strategy of calculating core polarizability is not highly accurate towards computing a total polarizability value. But this slight inaccuracy does not affect a calculated value of magic wavelength as the contribution of core polarizability to the total polarizabilities for the clock states is canceled to determine this wavelength. However, this inaccuracy can affect a tune-out wavelength, which is not more than ±1 Å for the calculated tune-out wavelengths discussed in the last paragraph of the present section. The comparison in Table I indicates 4.7% deviation for the $4^2D_{\frac{3}{2}}$ state, 4.9% deviation for the $4^2D_{\frac{5}{2}}$ state, and 3.8% deviation for the $5^2S_{\frac{1}{2}}$ state in the total static polarizability values.

TABLE I. Total static polarizabilities $\alpha_v(0)$ are presented in a.u. along with contributions from scalar $\alpha_v^{(0)}(0)$, core $\alpha_v^C(0)$, core-valence $\alpha_v^{VC}(0)$, and tensor $\alpha_v^{(2)}(0)$ parts. "Other" refers to the corresponding values obtained from the work of Safronova and Safronova [87]. "Our" refers to our calculated values which are rounded up to two decimal places.

State	$\alpha_v^{(0)}(0)$		$\alpha_v^C(0)$		$\alpha_v^{VC}(0)$		$\alpha_v^{(2)}(0)$		$\alpha_v(0)$	
	Our	Other	Our	Other	Our	Other	Our	Other	Our	Other
$4^2D_{\frac{3}{2}}$	6.89	6.742(26)	4.28	4.048	−0.33	−0.313	−3.48	−3.45(2)	7.36	7.03(4)
$4^2D_{\frac{5}{2}}$	6.93	6.815(32)	4.28	4.048	−0.36	−0.341	−4.86	−4.81(3)	5.99	5.71(4)
$5^2S_{\frac{1}{2}}$	42.07	40.64(17)	4.28	4.048	−0.17	−0.17	0.00	0.00	46.18	44.5(2)
$5^2P_{\frac{1}{2}}$	8.75		4.28		0.00		0.00		13.03	
$5^2P_{\frac{3}{2}}$	12.02		4.28		0.00		5.61		21.91	

We also present the static polarizabilities for $5^2P_{\frac{1}{2},\frac{3}{2}}$ states, which can be helpful in future experimental explorations of state-specific properties.

Figure 2 shows the wavelength dependency of the total polarizabilities for the $5^2S_{\frac{1}{2}}$ and $4^2D_{\frac{3}{2},\frac{5}{2}}$ states due to a linearly and a circularly polarized light. We consider right circularly polarized light [i.e., $\sigma = +1$ in Eq. (4)] in the present calculations of polarizabilities at the various M_{J_v} levels of the clock states. Here we choose the most important region of the electromagnetic spectrum from $\lambda = 77$ to 400 nm as there is no significant magic wavelength which can be prescribed for laser trapping purposes outside of this region. The entire spectrum of the wavelength as considered in all the four plots of Fig. 2 spans from the vacuum ultraviolet to the starting zone of the visible region. The peaks in the polarizability curves represent the resonances associated with the transitions $5^2S_{\frac{1}{2}} \to (5\text{–}7)^2P_{\frac{1}{2},\frac{3}{2}}$ and $4^2D_{\frac{3}{2},\frac{5}{2}} \to (5\text{–}7)^2P_{\frac{1}{2},\frac{3}{2}}$ and $(4\text{–}5)^2F_{\frac{5}{2},\frac{7}{2}}$. It is interesting to see that there is no resonance line in between 100 and 400 nm for $4D5_{(5/2)}$ (the $4^2D_{(J_v,M_{J_v})}$ state with $J_v = \frac{5}{2}$ and $M_{J_v} = \frac{5}{2}$) with a linearly polarized light [Fig. 2(b)]. This feature is a consequence of strong cancellation between scalar and tensor parts of the polarizability in that wavelength span. A similar characteristic for the resonance behavior of the $3D5_{(5/2)}$ state was seen in the recent work on dynamic polarizability for the Sc^{2+} ion [21]. Indeed, the resonances appear for this state when one considers circular polarization of light. The circular polarization induces the nonvanishing vector component, which is the sole reason for the occurrences of resonances in the polarizability profile of $4D5_{(5/2)}$.

The crossing points between the curves representing the dynamic polarizabilities of $5^2S_{\frac{1}{2}}$ and $4^2D_{\frac{3}{2},\frac{5}{2}}$ states in Fig. 2 show a number of magic wavelengths for the transitions between them. We find quite a few magic wavelengths

TABLE II. Contributions to $\alpha_v^V(0)$ (in a.u.) of the clock states from the intermediate states considered at the RCCSD(T), RMBPT(2), and DF levels.

State	RCCSD(T)	RMBPT(2)	DF
$4^2D_{\frac{3}{2}}$	3.40233	0.01070	0.00006
$4^2D_{\frac{5}{2}}$	2.05729	0.01265	0.00015
$5^2S_{\frac{1}{2}}$	42.07169	0.00089	0.00003

with high polarizability values at the mid-UV region (200–300 nm), and, therefore, these wavelengths can be very significant for the Y^{2+} clock experiment with the best possible precision. All the magic wavelengths within the range of 77 to 400 nm are presented in Table III with the corresponding polarizability values. This table also reveals the effect of the vector part of polarizability by comparing the results for the circularly polarized light with the results for a linearly polarized light. Here it is to be mentioned that the orientation of the polarization of light (σ) and the sign of M_{J_v} decide the resultant sign of the vector part of polarizability [see Eq. (4)]. This essentially means that the signs of these two factors (σ and M_{J_v}) are responsible apart from the sign of $\alpha_v^{(1)}(\omega)$ to determine whether there should be an additive or a subtractive effect to the total polarizability for a linearly polarized light to achieve the total polarizability for the circularly polarized light. Nevertheless, due to the presence of the vector part in the polarizability, the circularly polarized light provides a relatively greater number of magic wavelengths for the clock transitions and many of them are associated with large polarizability values. Moreover, both the values of the magic wavelengths and the corresponding polarizabilities are changed moderately in a few cases due to the change in light polarization from linear and circular. This facilitates external control on slight tuning of the magic wavelengths. Since the wavelengths of the transitions $5^2S_{\frac{1}{2}}\text{–}4^2D_{\frac{3}{2},\frac{5}{2}}$ are 1339.2 and 1483.0 nm, respectively, all the magic wavelengths presented in the table support the blue-detuned trapping scheme.

B. Dynamic polarizabilities and magic wavelengths for hyperfine-structure states

Instead of considering the electronic fine-structure transitions, experimentalists prefer to consider hyperfine transitions in most cases of trapping and cooling processes. Therefore, it may be physically more meaningful to estimate the magic wavelengths for the transitions between different hyperfine levels of the clock states.

The hyperfine-structure constant A values for nine low-lying states of Y^{2+} are calculated using the RCCSD(T) method and presented in Table IV. In order to calculate these constants, we choose the most abundant isotope of Y with mass number 89, nuclear spin $(I) = 1/2$, and nuclear magnetic moment $(\mu) = -0.137\,415\,4\ \mu_N$. The nuclear charge distribution of this isotope is assumed to have the Fermi-type form [89]. We compare the present RCCSD(T) values with

TABLE III. Magic wavelengths λ_{magic} (in nm) with corresponding polarizabilities α_{magic} (in a.u.) for $5^2S_{\frac{1}{2}}$ to $4^2D_{\frac{3}{2}}$ and $5^2S_{\frac{1}{2}}$ to $4^2D_{\frac{5}{2}}$ transitions due to linearly and circularly polarized ($\sigma = +1$) light. Notation (J_v, M_{J_v})–$(J'_v, M_{J'_v})$ in the second row indicates the transition $5^2S_{(J_v, M_{J_v})}$–$4^2D_{(J'_v, M_{J'_v})}$.

	Linearly polarized		Circularly polarized							
	$(\frac{1}{2}, \frac{1}{2})$–$(J'_v, M_{J'_v})$		$(\frac{1}{2}, -\frac{1}{2})$–$(J'_v, -M_{J'_v})$		$(\frac{1}{2}, -\frac{1}{2})$–$(J'_v, M_{J'_v})$		$(\frac{1}{2}, \frac{1}{2})$–$(J'_v, -M_{J'_v})$		$(\frac{1}{2}, \frac{1}{2})$–$(J'_v, M_{J'_v})$	
$(J'_v, M_{J'_v})$	λ_{magic}	α_{magic}	λ_{magic}	α_{magic}	λ_{magic}	α_{magic}	λ_{magic}	α_{magic}	λ_{magic}	α_{magic}
$(\frac{3}{2}, \frac{3}{2})$	293.77	9.57	294.83	22.16	294.77	−3.11	286.02	24.91	286.00	−5.11
			244.18	−97.23	247.36	−107.53	244.12	−116.35	246.54	−126.90
			226.14	−59.47	244.79	−98.92	232.54	−82.32	244.85	−119.02
			101.08	0.59			101.09	0.68		
	98.96	1.10	98.96	1.06	98.96	1.06	98.96	1.15	98.96	1.15
	85.39	4.52	85.31	3.35	85.35	5.79	85.50	3.36	85.61	5.22
	80.63	6.59	80.52	6.45	80.63	6.36	80.50	6.93	80.08	7.32
$(\frac{3}{2}, \frac{1}{2})$	293.84	28.79	294.85	32.99	294.83	24.58	286.02	36.85	286.02	26.85
	244.26	−107.13	244.32	−97.61	244.20	−97.30	244.29	−116.94	244.16	−116.45
	233.83	−78.13	226.68	−60.24	230.62	−67.61	227.31	−70.05	231.99	−81.06
	98.96	1.10	98.96	1.06	98.96	1.06	98.96	1.14	98.96	1.14
	85.38	3.88	85.73	3.07	85.80	3.48	85.16	3.81	85.44	4.23
	80.63	6.59	80.63	6.36	80.63	6.36	80.63	6.82	80.63	6.83
$(\frac{5}{2}, \frac{5}{2})$	293.75	6.26	294.83	19.71	294.77	−7.21	286.02	22.18	286.00	−9.64
			238.33	−81.99	246.62	−105.03	238.26	−96.02	245.47	−121.85
			229.28	−64.40	239.15	−83.97	230.70	−76.69	239.23	−99.04
			113.16	−0.82			112.17	−0.95		
			100.53	0.72	100.40	0.75	100.53	0.81	100.40	0.83
	99.54	0.98	99.30	0.99			99.30	1.07		
	85.40	5.04	98.63	1.13	86.15	5.57	98.63	1.22	86.22	5.42
	81.02	6.28	88.78	3.67	80.99	6.08	88.86	3.69	80.99	6.53
$(\frac{5}{2}, \frac{3}{2})$	293.82	21.05	294.85	28.94	294.81	12.81	286.02	32.16	286.00	13.07
	233.91	−78.33	234.17	−73.14	233.72	−72.19	234.14	−84.68	233.69	−83.47
	229.71	−69.82	222.72	−54.69	232.28	−69.59	224.60	−64.94	232.91	−81.69
	99.54	0.98	99.38	0.97	100.78	0.66	99.38	1.06	100.25	0.87
	85.40	4.65	85.73	3.08	85.99	4.64	85.04	3.62	85.89	4.92
	81.02	6.28	81.08	6.01	81.00	6.07	81.08	6.46	81.00	6.52
$(\frac{5}{2}, \frac{1}{2})$	293.87	28.44	294.85	30.87	294.83	25.50	286.02	33.97	286.02	27.61
	233.99	−78.51	234.05	−72.89	233.95	−72.67	234.03	−84.39	233.93	−84.11
	225.48	−62.52	222.50	−54.40	226.83	−60.48	224.26	−64.35	227.71	−70.62
	99.54	0.98	99.47	0.95	99.66	0.91	99.47	1.03	99.66	1.00
	85.39	4.46	85.79	3.43	85.88	3.94	85.37	4.13	85.62	4.52
	81.02	6.28	81.03	6.05	81.02	6.06	81.03	6.50	81.02	6.51

TABLE IV. Hyperfine A constants and hyperfine splitting in MHz.

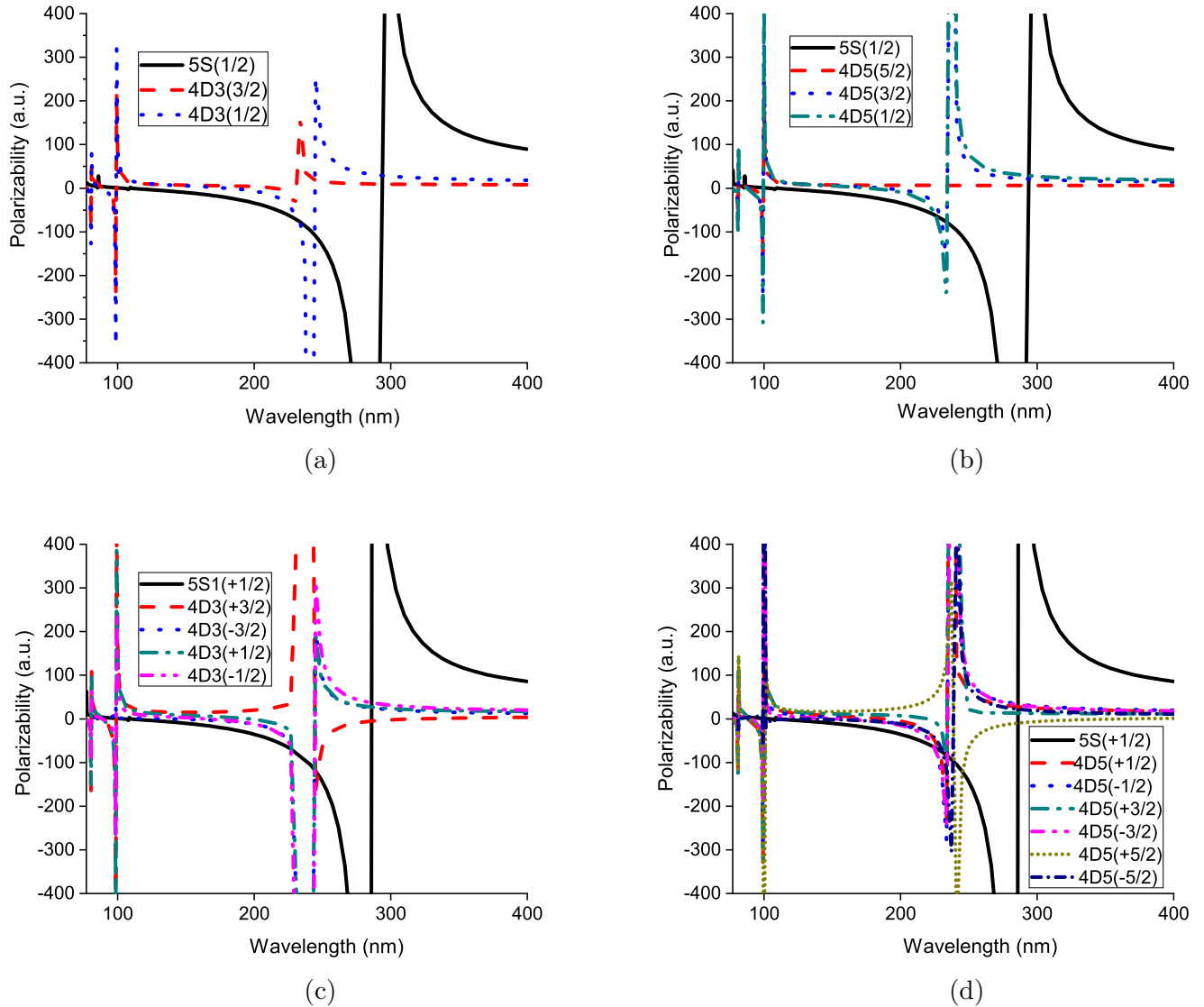| State	Hyperfine A constant				$F_1 \rightarrow F_2$	Hyperfine splitting	
	DF	RCCSD(T)	Other [39]			RCCSD(T)	Other [57]
			MCDF	Exp.			
$4^2D_{\frac{3}{2}}$	79.55	102.74			$2 \rightarrow 1$	205.47	
$4^2D_{\frac{5}{2}}$	33.20	14.25			$3 \rightarrow 2$	42.74	
$4^2F_{\frac{5}{2}}$	0.48	0.86			$3 \rightarrow 2$	2.59	
$4^2F_{\frac{7}{2}}$	−0.27	−0.88			$4 \rightarrow 3$	3.52	
$5^2S_{\frac{1}{2}}$	1441.92	1793.19	1780	1803(5)	$1 \rightarrow 0$	1793.19	1920 ± 150
$5^2P_{\frac{1}{2}}$	284.44	371.47	352	391(5)	$1 \rightarrow 0$	371.47	
$5^2P_{\frac{3}{2}}$	49.57	73.86			$2 \rightarrow 1$	147.72	128
$5^2D_{\frac{3}{2}}$	17.12	21.63			$2 \rightarrow 1$	43.25	
$5^2D_{\frac{5}{2}}$	7.19	8.10			$3 \rightarrow 2$	24.29	

FIG. 2. The variations of total polarizabilities (indicated by polarizability) with wavelengths for the states $5^2S_{\frac{1}{2}}$ and $4^2D_{\frac{3}{2},\frac{5}{2}}$ to extract magic wavelengths for the transitions between them. (a, b) Linearly polarized light. (c, d) Circularly polarized light. Here the different (J_v, M_{J_v}) levels of the state $n^2L_{J_v}$ are indicated by $nL2J_v(M_{J_v})$ with n the principal quantum number of the valence orbital and L the orbital angular momentum quantum number of the ion.

the available hyperfine A values in the literature and find good agreement between them [39]. As the nuclear quadrupole moment is zero for a spin-half nucleus, the hyperfine shifts [see Eq. (14)] and consequently the splittings are calculated using hyperfine A constants only. The splitting values are displayed in the same table with comparison to a few very old experimental measurements [57]. This table also shows high values of relative correlation corrections to the hyperfine A constants of the $4^2D_{\frac{5}{2}}$ and $4^2F_{\frac{5}{2},\frac{7}{2}}$ states. This relative correlation correction is defined by $|\frac{\text{RCCSD(T) value} - \text{DF value}}{\text{DF value}}| \times 100$. From our investigation, we find strong core polarization effect [77] is the main reason for such high impact of correlation.

Figure 3 represents the variation profiles of dynamic polarizabilities for the hyperfine levels of the clock states within the same spectral region which is considered in Fig. 2. For the circularly polarized light with $\sigma = +1$, the polarizability pro-

files of $4^2D_{\frac{3}{2}}(F_v = 2, M_{F_v} = \pm 2)$, $4^2D_{\frac{5}{2}}(F_v = 3, M_{F_v} = \pm 3)$, and $5^2S_{\frac{1}{2}}(F_v = 1, M_{F_v} = \pm 1)$ states are same as the profiles of $4^2D_{\frac{3}{2}}(M_{J_v} = \pm \frac{3}{2})$, $4^2D_{\frac{5}{2}}(M_{J_v} = \pm \frac{5}{2})$, and $5^2S_{\frac{1}{2}}(M_{J_v} = \pm \frac{1}{2})$ states, respectively. This is because of the unit value of the multiplication factors in Eqs. (8) and (9) which relate $\alpha_{vF}^{(i)}(\omega)$ with $\alpha_v^{(i)}(\omega)$ for these states with $i = 1, 2$. Also the polarizability values are same for $4^2D_{\frac{3}{2}}(F_v = 2, M_{F_v} = 0)$ and $4^2D_{\frac{3}{2}}(F_v = 1, M_{F_v} = 0)$ states. We have not shown the dynamic profile of the states separately in the figure for which the profiles are the same.

In Table V, we tabulate the magic wavelengths due to the transitions between the hyperfine levels of the clock states for linearly and circularly polarized light. Similar to Table III, we get a few more magic wavelengths for the circularly polarized light compared to the linearly polarized light due to the
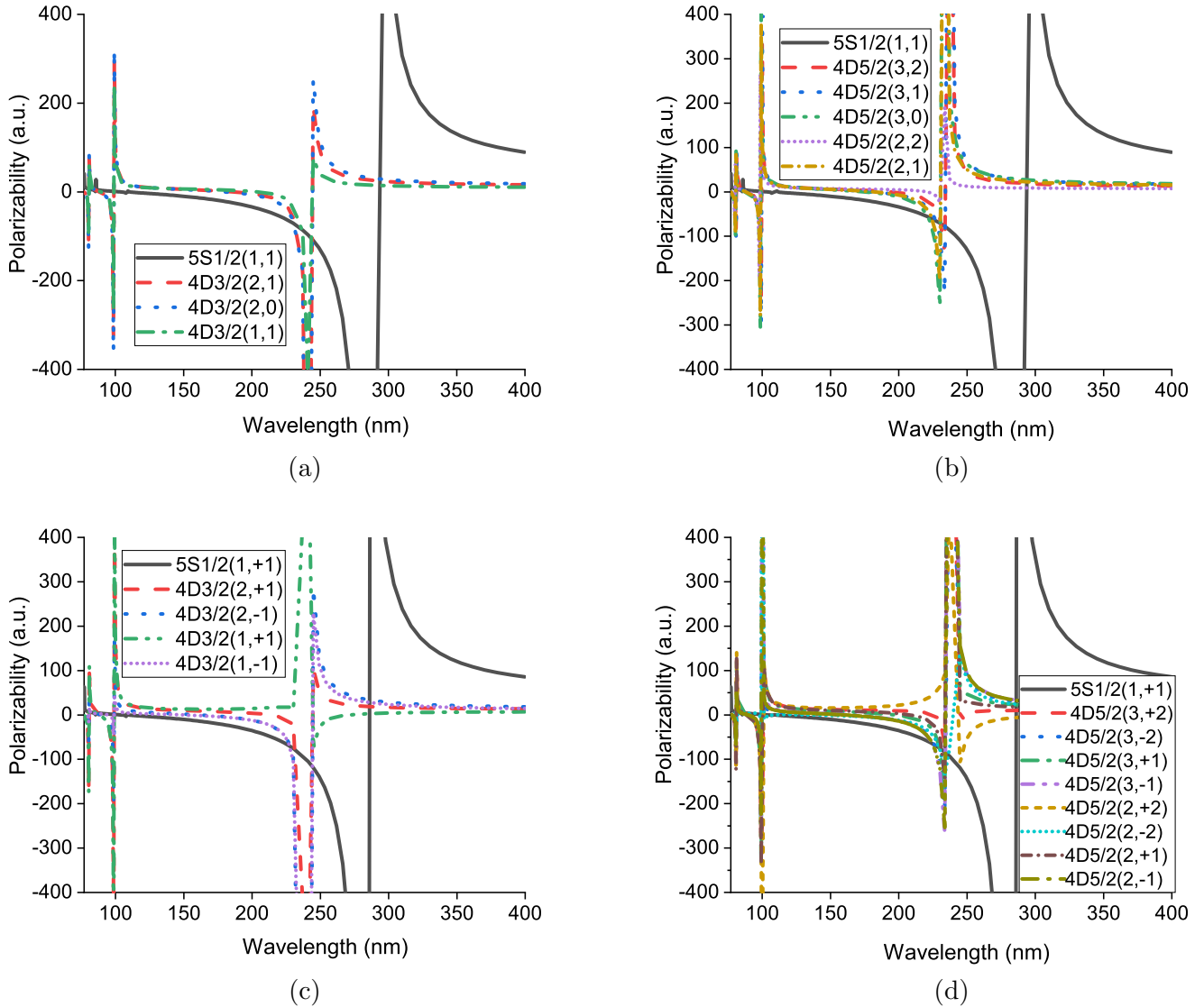
FIG. 3. Representation of Fig. 2, but now by including the effect of hyperfine splittings in the fine-structure states $5^2S_{\frac{1}{2}}$ and $4^2D_{\frac{3}{2},\frac{5}{2}}$. (a, b) Linearly polarized light. (c, d) Circularly polarized light. Here the different (F_v, M_{F_v}) levels of the state $n^2L_{J_v}$ are indicated by $nLJ_v(F_v, M_{F_v})$ with n the principal quantum number of the valence orbital and L the orbital angular momentum quantum number of the ion.

presence of vector part of valence polarizability in the former. From a comparison between Tables V and III, it is obvious that the hyperfine splitting can induce small but noticeable changes both in the magic wavelengths and the corresponding polarizabilities with more degrees of freedom in the choices of (F_v, M_{F_v}) combinations for each (J_v, M_{J_v}).

In order to calculate theoretical uncertainties in the RCCSD(T) hyperfine A values in Table IV, we classify atomic states of Y^{2+} in two different classes. One class (class I) has the correlation correction by less than 50%: $4^2D_{\frac{3}{2}}$, $5^2S_{\frac{1}{2}}$, $5^2P_{\frac{1}{2}}$, $5^2P_{\frac{3}{2}}$, and $5^2D_{\frac{3}{2}}$. The second class (class II) has it by more than 50%: $4^2D_{\frac{5}{2}}$, $4^2F_{\frac{5}{2}}$, and $4^2F_{\frac{7}{2}}$. We believe the uncertainties in the hyperfine values are dominated by the uncertainties in the correlation corrections computed by our present RCCSD(T) method. Therefore, the uncertainties in the class II states are supposed to be higher than the uncertainties in the class I states. There can be a small amount

of uncertainties in the DF values as well, which we can approximately calculate by comparing the expectation values of $1/r$ for these states as computed by using our optimized GTO basis functions and as obtained by using the numerical DF wave functions of the GRASP92 code [90]. The $1/r$ values can certainly be one of the parameters to judge the accuracy of the DF wave functions near to the nuclear region where the hyperfine values are peaked. Nevertheless, as far as the correlation is concerned, the spread in the correlation corrections and, therefore, in the total hyperfine values can be roughly estimated by comparing the present RCCSD(T) values with the corresponding values obtained from another similar method such as SDpT (linearized coupled cluster with single, double, and partial triple corrections) [91,92], which can also provide very highly accurate results [10]. However, for Y^{2+}, no such SDpT hyperfine values are available to our knowledge. Therefore, we calculate the hyperfine values for Sr^+, which is also an element of a Rb-isoelectronic sequence

TABLE V. Magic wavelengths λ_{magic} (in nm) with corresponding total polarizabilities α_{magic} (in a.u.) for the $5^2S_{\frac{1}{2}}$–$4^2D_{\frac{3}{2},\frac{5}{2}}$ transitions for linearly and circularly polarized ($\sigma = +1$) lights. Notation (F_v, M_{F_v})–$(F'_v, M_{F'_v})$ in the second row indicates the transition $5^2S_{(J_v, M_{J_v})}(F_v, M_{F_v})$–$4^2D_{(J'_v, M_{J'_v})}(F'_v, M_{F'_v})$.

| | Linearly polarized | | Circularly polarized | | | | | | | |
| | $(1, 1)$–$(F'_v, M_{F'_v})$ | | $(1, -1)$–$(F'_v, -M_{F'_v})$ | | $(1, -1)$–$(F'_v, M_{F'_v})$ | | $(1, 1)$–$(F'_v, -M_{F'_v})$ | | $(1, 1)$–$(F'_v, M_{F'_v})$ | |
$[J'_v](F'_v, M_{F'_v})$	λ_{magic}	α_{magic}	λ_{magic}	α_{magic}	λ_{magic}	α_{magic}	λ_{magic}	α_{magic}	λ_{magic}	α_{magic}
$[\frac{3}{2}]$ (2,2)	293.77	9.57	294.83	22.16	294.77	−3.11	286.02	24.91	286.00	−5.11
			244.18	−97.23	247.36	−107.53	244.12	−116.35	246.54	−126.90
			226.14	−59.47	244.79	−98.92	232.54	−82.32	244.85	−119.02
			101.08	0.59			101.09	0.68		
	98.96	1.10	98.96	1.06	98.96	1.06	98.96	1.15	98.96	1.15
	85.39	4.52	85.31	3.35	85.35	5.79	85.50	3.36	85.61	5.22
	80.63	6.59	80.52	6.45	80.63	6.36	80.50	6.93	80.08	7.32
$[\frac{3}{2}]$, (2,1)	293.85	24.2	294.88	30.28	294.85	17.66	286.03	32.76	286.00	18.86
	244.19	−106.87	244.30	−97.55	243.93	−96.51	244.27	−116.84	243.82	−115
	231.91	−74.45	226.53	−60.02	227.81	−62.45	226.97	−69.28	237.54	−93.76
	98.96	1.10	98.97	1.06	98.96	1.06	99.41	1.05	98.96	1.14
	85.38	4.06	85.30	3.53	85.34	4.71	85.51	3.44	85.56	4.28
	80.63	6.59	80.63	6.36	80.63	6.36	81.06	6.48	80.63	6.83
$[\frac{3}{2}]$, (2/1,0)	293.87	29.07								
	244.27	−107.13								
	230.62	−71.63								
	98.96	1.10								
	85.36	3.92								
	80.63	6.59								
$[\frac{3}{2}]$, (1,1)	293.81	14.45	294.86	24.87	294.82	3.82	286.03	27.89	286.02	2.88
	243.55	−104.76	244.24	−97.36			244.20	−116.56		
	237.45	−86.66	226.26	−59.63			226.74	−68.71		
	98.96	1.10	98.97	1.06	98.96	1.06	98.97	1.14	98.96	1.15
	85.39	4.36	85.34	3.40	85.37	5.38	85.50	3.36	85.60	4.91
	80.63	6.59	84.20	3.78			84.66	3.61		
			82.05	5.34			81.71	6.00		
			80.66	6.34	80.63	6.36	80.66	6.80	80.63	6.82
$[\frac{5}{2}]$, (3,3)	293.75	6.26	294.83	19.71	294.77	−7.21	286.02	22.18	286.00	−9.64
			238.33	−81.99	246.62	−105.03	238.26	−96.02	245.47	−121.85
			229.28	−64.40	239.15	−83.97	230.70	−76.69	239.23	−99.04
			113.16	−0.82			112.17	−0.95		
			100.53	0.72	100.40	0.75	100.53	0.81	100.40	0.83
	99.54	0.98	99.30	0.99			99.30	1.07		
	85.40	5.04	98.63	1.13	86.15	5.57	98.63	1.22	86.22	5.42
	81.02	6.28	88.78	3.67	80.99	6.08	88.86	3.69	80.99	6.53
$[\frac{5}{2}]$, (3,2)	293.81	18.59	294.83	26.81	294.81	10.07	286.02	29.79	286.00	9.99
	233.86	−78.21	234.20	−73.18	243.21	−94.54	234.15	−84.70	242.84	−111.49
	230.63	−71.59	224.20	−56.72	240.77	−87.79	226.17	−67.66	240.82	−103.99
	98.89	0.98	99.37	0.97	99.62	0.92	98.72	1.06	99.62	0.86
	84.92	4.71	85.35	3.37	85.37	5.06	85.02	3.28	85.15	5.55
	80.59	6.28	81.09	6.00	80.57	6.41	80.67	6.45	80.57	6.52
$[\frac{5}{2}]$, (3,1)	293.86	25.97	294.87	29.59	294.85	17.04	286.03	33.37	286.02	22.76
	233.98	−78.47	234.13	−73.03	233.82	−72.39	234.07	−84.46	233.87	−83.94
	227.00	−64.97	222.65	−54.59	230.73	−66.81	224.38	−64.53	230.15	−75.42
	99.54	0.98	99.41	0.96	100.09	0.81	99.44	1.04	99.80	0.97
	85.39	4.54	85.36	3.59	85.38	5.66	85.52	3.63	85.59	4.83
	81.02	6.28	81.06	6.03	81.01	6.07	81.04	6.49	81.01	6.52
$[\frac{5}{2}]$, (3/2,0)	293.87	27.06								
	230.46	−71.22								
	221.19	−56.04								
	98.90	1.12								
	85.38	3.62								

TABLE V. *(Continued).*

| | Linearly polarized | | Circularly polarized | | | | | | | |
| | (1, 1)–(F'_v, M_F'_v) | | (1,−1)–(F'_v, −M_F'_v) | | (1,−1)–(F'_v, M_F'_v) | | (1, 1)–(F'_v, −M_F'_v) | | (1, 1)–(F'_v, M_F'_v) | |
$[J'_v](F'_v, M_{F'_v})$	λ_{magic}	α_{magic}	λ_{magic}	α_{magic}	λ_{magic}	α_{magic}	λ_{magic}	α_{magic}	λ_{magic}	α_{magic}
	80.59	6.62								
$[\frac{5}{2}]$, (2,2)	293.79	8.72	294.86	21.25	294.81	−3.87	286.02	23.85	286.01	−5.86
			237.43	−79.84	245.50	−101.19	237.35	−93.14	244.83	−118.97
			227.89	−62.16	239.63	−85.05	229.69	−74.52	239.69	−100.44
			110.77	0.24			109.63	0.10		
			106.08	−0.89			106.28	−0.80		
	99.54	0.98	97.78	1.32	100.39	0.75	97.76	1.40	99.99	0.92
	85.40	4.97	89.74	3.32	85.39	7.05	89.93	3.33	85.68	6.37
	81.02	6.28	85.33	2.91	80.99	6.08	85.48	2.93	80.99	6.53
$[\frac{5}{2}]$, (2,1)	293.85	22.44	294.87	29.59	294.85	17.04	286.03	32.76	286.02	17.92
	230.42	−71.14	234.13	−73.03	233.82	−72.39	234.10	−84.55	233.79	−83.73
	224.08	−60.28	222.65	−54.59	230.73	−66.81	224.49	−64.73	231.16	−77.72
	98.90	1.12	98.76	0.96	99.61	0.81	98.76	1.05	99.61	0.90
	85.38	3.83	84.85	3.62	84.87	5.73	85.03	3.44	85.13	5.13
	80.59	6.62	80.63	6.03	80.58	6.07	80.63	6.48	80.58	6.52

like Y^{2+}, by the present RCCSD(T) method and compare these values with the corresponding hyperfine values as calculated by the SDpT method of Safronova [91]. Such a comparison is available for few states in [10]. Nevertheless, we find maximum discrepancy of 1.8% in the comparison for all the states belong to class I. Our observations and experience of calculating hyperfine values for the isoelectronic sequence of alkali-metal-like atoms [10,82,93] indicate that for these states the discrepancy should not be more than $\pm1.8\%$ for Y^{2+}, which is more ionized than Sr^+. This is mainly due to the fact that with increasing ionization in a particular isoelectronic sequence the correlation correction decreases [82,83], and RCCSD(T) and SDpT or SD (SDpT without partial triple) values approach towards more and more close agreement usually [93]. Therefore, we can assume maximum uncertainty of $\pm2\%$ for the hyperfine values of class I states of Y^{2+} due to discrepancy in correlation correction. However, for class II states, for which the correlation correction discrepancy between RCCSD(T) and SDpT or SD methods decreases from singly to doubly ionized systems along an isoelectronic sequence of an alkali-metal atom [93], a different strategy is considered. Here we compare the correlation correction in the hyperfine value of the $4^2D_{\frac{5}{2}}$ state as calculated by the present RCCSD(T) method and as calculated by the SDpT method of Safronova for Sr^+ [91]. We find discrepancy of around 5% in this correlation value. Now for Y^{2+}, which is more ionized than Sr^+, this discrepancy is expected to be lower than 5%; even then, let us assume that this discrepancy is still 5% for the purpose of calculating uncertainty. This 5% discrepancy in correlation can invoke an uncertainty of around $\pm7\%$ in the RCCSD(T) hyperfine value of the $4^2D_{\frac{5}{2}}$ state of Y^{2+}. Now as for $4^2F_{\frac{5}{2}}$ and $4^2F_{\frac{7}{2}}$ states no SDpT values are available in the work of Safronova for Sr^+, it is very difficult to compute the uncertainty values for these two states. Therefore, with a very rough assumption, if we assume the same amount of 5% uncertainty in the correlation corrections of $4^2F_{\frac{5}{2}}$ and $4^2F_{\frac{7}{2}}$ states hold as well for the Sr^+

ion, then one should not expect uncertainties by more than $\pm7\%$ in the RCCSD(T) hyperfine values for these two states of Y^{2+} also. Therefore, accounting for the preciseness of DF wave functions near to the nuclear region and approximate contributions from the Breit interactions [83], and from a comparative assessment between the RCCSD(T) and SDpT results for Sr^+, we estimate the theoretical uncertainties in the RCCSD(T) hyperfine A values in Table IV of around $\pm3\%$ for the class I states and $\pm8\%$ for the class II states.

To estimate uncertainty in the calculated magic wavelengths for Y^{2+}, we reevaluate the magic wavelengths by replacing only our calculated RCCSD(T) dipole matrix elements by the corresponding available dipole matrix elements in the literature [87] which were calculated by using an all-order RMBPT method. The transition matrix elements which we find in their work [87] are $5^2S_{\frac{1}{2}}$–$5^2P_{\frac{1}{2}, \frac{3}{2}}$, $4^2D_{\frac{3}{2}, \frac{5}{2}}$–$n^2P_{\frac{1}{2}, \frac{3}{2}}$ with $n = 5$–7, and $4^2D_{\frac{3}{2}, \frac{5}{2}}$–$m^2F_{\frac{5}{2}, \frac{7}{2}}$ with $m = 4$–6. The maximum difference between these recalculated magic wavelengths and the corresponding magic wavelengths presented in Tables III and V is considered as the uncertainty in the latter values, which is estimated around $\pm1\%$.

C. Tune-out wavelengths for $4^2D_{\frac{3}{2}, \frac{5}{2}}$ and $5^2S_{\frac{1}{2}}$ states for a linearly polarized light

We also report a few tune-out wavelengths in Table VI for the hyperfine levels of the $5^2S_{\frac{1}{2}}$ and $4^2D_{\frac{3}{2}, \frac{5}{2}}$ states of Y^{2+}. In this table, we consider a linearly polarized light only. There is an advantage of calculating tune-out wavelengths for a linearly polarized light. Table VI displays the wavelength at which the total polarizability of a particular hyperfine state becomes zero for a linearly polarized light. However, due to the nonzero vector polarizability contribution, the total polarizability for a circularly polarized light does not become zero at the same wavelength for the same hyperfine state. As an example, the vector contributions to the total polarizability of the ground state $4^2D_{\frac{3}{2}}$ with $F_v = 2$ and $M_{F_v} = \pm2$ at the

TABLE VI. Tune-out wavelengths (in nm) for Y^{2+} at the hyperfine levels (F_v, M_{F_v}).

$5^2S_{\frac{1}{2}}$	$4^2D_{\frac{3}{2}}$				$4^2D_{\frac{5}{2}}$					
(1,1)	(2,2)	(2,1)	(2 or 1, 0)	(1,1)	(3,3)	(3,2)	(3,1)	(3 or 2,0)	(2,2)	(2,1)
293.73	230.83	244.46	244.47	244.36	99.54	234.14	234.15	230.59	230.50	230.59
108.68	215.32	186.85	180.59	204.41	91.04	193.06	180.46	175.24	220.54	181.86
	98.96	98.96	98.96	98.96		99.54	99.54	98.90	98.89	98.97
	90.01	88.02	88.02	89.38		89.19	88.45	87.74	90.06	88.16
	80.61	80.62	80.62	80.62	81.00	81.00	81.01	80.58	80.57	80.58

tune-out wavelengths 230.83 and 215.32 nm become 414.14 and 25.84 a.u., respectively, whereas, for the $F_v = 1$ and $M_{F_v} = \pm 1$ hyperfine component of the same fine-structure state, the vector polarizability values become 53.86 and 14.98 a.u. at the presented tune-out wavelengths 244.36 and 204.41 nm, respectively. These values can be used to calculate fictitious magnetic field induced by the circular polarization of light [94]. The prior knowledge of the zero Stark-shift wavelengths for a particular atomic state can be advantageous for an accurate trap-insensitive experimental measurement [5,95,96].

IV. CONCLUSION

In the present paper, we have determined the magic wavelengths corresponding to the $5^2S_{\frac{1}{2}}$–$4^2D_{\frac{3}{2},\frac{5}{2}}$ clock transitions of $^{89}Y^{2+}$ for two different types of polarization (linear and circular) of the projected light beam. The magic wavelengths span from the vacuum ultraviolet to the near ultraviolet region of the electromagnetic spectrum. The data are presented both at the fine-structure and the associated hyperfine levels of the atomic states, and this gives an understanding of how much the hyperfine interaction can affect the magic trapping conditions viable for the fine-structure states. Indeed we have found slight modifications in the magic wavelength values after imposing hyperfine splitting on the fine-structure clock states. But most importantly, the number of magic wavelengths is increased. Many of these magic wavelengths can have potential applications for trap-related experimental explorations. Irrespective of the nature of the polarization of light, our calculations show that the polarizabilities at the magic wavelengths between 200 and 300 nm are higher and, thus, these wavelengths are more important for the experimental purposes. The calculated tune-out wavelengths in the present paper have important applications to perform trap-insensitive experiments. Also, we demonstrate quantitatively the advantage of using a circularly polarized light which yields extra trapping potential from the vector part of the polarizability. The calculated static polarizabilities for $4^2D_{\frac{3}{2},\frac{5}{2}}$, $5^2S_{\frac{1}{2}}$, and $5^2P_{\frac{1}{2},\frac{3}{2}}$ states are useful to calculate the blackbody radiation shifts of the transition frequencies among these states at a definite temperature. The hyperfine constants for most of the states of $^{89}Y^{2+}$ are reported for the first time in the literature to the best of our knowledge.

[1] J. McKeever, J. R. Buck, A. D. Boozer, A. Kuzmich, H.-C. Nägerl, D. M. Stamper-Kurn, and H. J. Kimble, Phys. Rev. Lett. **90**, 133602 (2003).

[2] M. S. Safronova, U. I. Safronova, and C. W. Clark, Phys. Rev. A **87**, 052504 (2013).

[3] J. Roßnagel, K. N. Tolazzi, F. Schmidt-Kaler, and K. Singer, New J. Phys. **17**, 045004 (2015).

[4] W. F. Holmgren, R. Trubko, I. Hromada, and A. D. Cronin, Phys. Rev. Lett. **109**, 243004 (2012).

[5] R. H. Leonard, A. J. Fallon, C. A. Sackett, and M. S. Safronova, Phys. Rev. A **92**, 052501 (2015); **95**, 059901(E) (2017).

[6] A. V. Gorshkov, A. M. Rey, A. J. Daley, M. M. Boyd, J. Ye, P. Zoller, and M. D. Lukin, Phys. Rev. Lett. **102**, 110503 (2009).

[7] V. V. Flambaum, V. A. Dzuba, and A. Derevianko, Phys. Rev. Lett. **101**, 220801 (2008).

[8] M. G. Kozlov, M. S. Safronova, J. R. Crespo López-Urrutia, and P. O. Schmidt, Rev. Mod. Phys. **90**, 045005 (2018).

[9] S. G. Porsev, K. Beloy, and A. Derevianko, Phy. Rev. Lett. **102**, 181601 (2009).

[10] N. N. Dutta and S. Majumder, Phys. Rev. A **90**, 012522 (2014).

[11] H. Häffner, C. F. Roos, and R. Blatt, Phys. Rep. **469**, 155 (2008).

[12] B. Lekitsch, S. Weidt, A. G. Fowler, K. Mølmer, S. J. Devitt, C. Wunderlich, and W. K. Hensinger, Sci. Adv. **3**, e1601540 (2015).

[13] G. W. Biedermann, X. Wu, L. Deslauriers, S. Roy, C. Mahadeswaraswamy, and M. A. Kasevich, Phys. Rev. A **91**, 033629 (2015).

[14] R. Charriere, M. Cadoret, N. Zahzam, Y. Bidel, and A. Bresson, Phys. Rev. A **85**, 013639 (2012).

[15] B. Dubetsky and M. A. Kasevich, Phys. Rev. A **74**, 023615 (2006).

[16] Y. M. Yu and B. K. Sahoo, Phys. Rev. A **97**, 041403(R) (2018).

[17] C. W. Chou, D. B. Hume, J. C. J. Koelemeij, D. J. Wineland, and T. Rosenband, Phys. Rev. Lett. **104**, 070802 (2010).

[18] P. Dubé, A. A. Madej, M. Tibbo, and J. E. Bernard, Phys. Rev. Lett. **112**, 173002 (2014).

[19] N. Huntemann, C. Sanner, B. Lipphardt, C. Tamm, and E. Peik, Phys. Rev. Lett. **116**, 063001 (2016).

[20] A. Kozlov, V. A. Dzuba, and V. V. Flambaum, Phys. Rev. A **88**, 032509 (2013).

[21] N. N. Dutta, S. Roy, and P. C. Deshmukh, Phys. Rev. A **92**, 052510 (2015).

[22] A. Derevianko, V. A. Dzuba, and V. V. Flambaum, Phys. Rev. Lett. **109**, 180801 (2012).

[23] U. Dammalapati, K. Harada, and Y. Sakemi, Phys. Rev. A **93**, 043407 (2016).

[24] R. C. Brown, N. B. Phillips, K. Beloy, W. F. McGrew, M. Schioppo, R. J. Fasano, G. Milani, X. Zhang, N. Hinkley, H. Leopardi, T. H. Yoon, D. Nicolodi, T. M. Fortier, and A. D. Ludlow, Phys. Rev. Lett. **119**, 253001 (2017).

[25] J. Kaur, S. Singh, B. Arora, and B. K. Sahoo, Phys. Rev. A **92**, 031402(R) (2015).

[26] A. Roy, S. De, B. Arora, and B. K. Sahoo, J. Phys. B **50**, 205201 (2017).

[27] P.-L. Liu, Y. Huang, W. Bian, H. Shao, H. Guan, Y.-B. Tang, C.-B. Li, J. Mitroy, and K.-L. Gao, Phys. Rev. Lett. **114**, 223001 (2015).

[28] H. Katori, K. Hashiguchi, E. Yu. Il'inova, and V. D. Ovsiannikov, Phys. Rev. Lett. **103**, 153004 (2009).

[29] A. Bhowmik, N. N. Dutta, and S. Majumder, Phys. Rev. A **97**, 022511 (2018).

[30] C. Tamm, N. Huntemann, B. Lipphardt, V. Gerginov, N. Nemitz, M. Kazda, S. Weyers, and E. Peik, Phys. Rev. A **89**, 023820 (2014).

[31] A. D. Ludlow, M. M. Boyd, J. Ye, E. Peik, and P. O. Schmidt, Rev. Mod. Phys. **87**, 637 (2015).

[32] H. S. Margolis, G. P. Barwood, G. Huang, H. A. Klein, S. N. Lea, K. Szymaniec, and P. Gill, Science **306**, 1355 (2004).

[33] W. Oskey, Phys. Rev. Lett. **97**, 020801 (2006).

[34] G. P. Barwood, G. Huang, H. A. Klein, L. A. M. Johnson, S. A. King, H. S. Margolis, K. Szymaniec, and P. Gill, Phys. Rev. A **89**, 050501(R) (2014).

[35] C. D. Bruzewicz, J. Chiaverini, R. McConnell, and J. M. Sage, Appl. Phys. Rev. **6**, 021314 (2019).

[36] M. Brownnutt, ^{88}Sr$^+$ ion trapping techniques and technologies for quantum information processing, Ph.D. dissertation, Imperial College London, 2007.

[37] A. M. Eltony, D. Gangloff, M. Shi, A. Bylinskii, V. Vuletić, and I. L. Chuang, Quantum Inf. Process. **15**, 5351 (2016).

[38] M. Schwarz, O. O. Versolato, A. Windberger, F. R. Brunner, T. Ballance, S. N. Eberle, J. Ullrich, P. O. Schmidt, A. K. Hansen, A. D. Gingell, M. Drewsen, and J. R. Crespo López-Urrutia, Rev. Sci. Instrum. **83**, 083115 (2012).

[39] L. J. Vormawah, M. Vilén, R. Beerwerth, P. Campbell, B. Cheal, A. Dicker, T. Eronen, S. Fritzsche, S. Geldhof, A. Jokinen, S. Kelly, I. D. Moore, M. Reponen, S. Rinta-Antila, S. O. Stock, and A. Voss, Phys. Rev. A **97**, 042504 (2018).

[40] J. Mitroy, M. S. Safronova, and C. W. Clark, J. Phys. B **43**, 202001 (2010).

[41] R. Trubko, J. Greenberg, M. T. St. Germaine, M. D. Gregoire, W. F. Holmgren, I. Hromada, and A. D. Cronin, Phys. Rev. Lett. **114**, 140404 (2015).

[42] A. Das, A. Bhowmik, N. N. Dutta, and S. Majumder, J. Phys. B **51**, 025001 (2018).

[43] T. Meguro, T. Caughey, L. Wolf, and Y. Aoyagi, Opt. Lett. **19**, 102 (1994).

[44] H. Kumagai, IEEE J. Sel. Top. Quantum Electron. **10**, 1252 (2004).

[45] *Excimer Laser Technology*, edited by D. Basting and G. Marowsky (Springer-Verlag, Berlin, 2005).

[46] J. Sakuma, K. Deki, A. Finch, Y. Ohsako, and T. Yokota, Appl. Opt. **39**, 5505 (2000).

[47] T. Uchimura, T. Onoda, C.-H. Lin, and T. Imasaka, Rev. Sci. Instrum. **70**, 3254 (1999).

[48] R. H. Lipson, S. S. Dimov, P. Wang, Y. J. Shi, D. M. Mao, and X. K. Hu, Instrum. Sci. Technol. **28**, 85 (2007).

[49] D. Jiang, B. Arora, M. S. Safronova, and C. W Clark, J. Phys. B **42**, 154020 (2009).

[50] E. J. Angstmann, V. A. Dzuba, and V. V. Flambaum, Phys. Rev. Lett. **97**, 040802 (2006).

[51] K. Beloy, U. I. Safronova, and A. Derevianko, Phys. Rev. Lett. **97**, 040801 (2006).

[52] G. Werth, Phys. Scr. **1995**, 206 (1995).

[53] D. Hucul, J. E. Christensen, E. R. Hudson, and W. C. Campbell, Phys. Rev. Lett. **119**, 100501 (2017).

[54] S. T. Maniak, L. J. Curtis, C. E. Theodosiou, R. Hellborg, S. G. Johansson, I. Martinson, R. E. Irving, and D. J. Beideck, Astron. Astrophys. **286**, 978 (1994).

[55] É. Biémont, K. Blagoev, L. Engström, H. Hartman, H. Lundberg, G. Malcheva, H. Nilsson, R. W. Blackwell, P. Palmeri, and P. Quinet, Mon. Not. R. Astron. Soc. **414**, 3350 (2011).

[56] T. Brage, G. M. Wahlgren, S. G. Johansson, D. S. Leckrone, and C. R. Proffitt, Astrophys. J. **496**, 1051 (1998).

[57] M. F. Crawford and N. Olson, Phys. Rev. **76**, 1528 (1949).

[58] F. L. Kien, P. Schneeweiss, and A. Rauschenbeutel, Eur. Phys. J. D **67**, 92 (2013).

[59] W. R. Johnson, Z. W. Liu, and J. Sapirstein, At. Data Nucl. Data Tables **64**, 279 (1996).

[60] I. P. Grant, *Relativistic Quantum Theory of Atoms and Molecules: Theory and Computation* (Springer, New York, 2007).

[61] *Modern Techniques in Computational Chemistry: MOTECC-90*, edited by E. Clementi (Springer, New York, 1990).

[62] M. S. Safronova and U. I. Safronova, Phys. Rev. A **83**, 052508 (2011).

[63] N. L. Manakov, V. D. Ovsiannikov, and L. P. Rapoport, Phys. Rep. **141**, 320 (1986).

[64] K. Beloy, Theory of the ac stark effect on the atomic hyperfine structure and applications to microwave atomic clocks, Ph.D. dissertation, University of Nevada, 2009.

[65] V. A. Dzuba, V. V. Flambaum, K. Beloy, and A. Derevianko, Phys. Rev. A **82**, 062513 (2010).

[66] J. Kaur, S. Singh, B. Arora, and B. K. Sahoo, Phys. Rev. A **95**, 042501 (2017).

[67] B. H. Bransden and C. J. Joachain, *Physics of Atoms and Molecules* (Pearson Education, Harlow, 2003).

[68] K. T. Cheng and W. J. Childs, Phys. Rev. A **31**, 2775 (1985).

[69] N. N. Dutta, S. Roy, G. Dixit, and S. Majumder, Phys. Rev. A **87**, 012501 (2013).

[70] R. K. Chaudhuri, B. K. Sahoo, B. P. Das, H. Merlitz, U. S. Mahapatra, and D. Mukherjee, J. Chem. Phys. **119**, 10633 (2003).

[71] K. Raghavachari, G. W. Trucks, J. A. Pople, and M. Head-Gordon, Chem. Phys. Lett. **157**, 479 (1989).

[72] M. Reiher and B. Hess, *Modern Methods and Algorithms of Quantum Chemistry* (NIC, Jülich, 2000), Vol. 3, p. 479.

[73] I. Lindgren and J. Morrison, *Atomic Many-Body Theory* (Springer-Verlag, Berlin, 1986).

[74] I. Shavitt and R. J. Bartlett, *Many-Body Methods in Chemistry and Physics: MBPT and Coupled-Cluster Theory* (Cambridge University, Cambridge, England, 2009).

[75] I. Lindgren and D. Mukherjee, Phys. Rep. **151**, 93 (1987).

[76] N. N. Dutta and S. Majumder, Indian J. Phys. **90**, 373 (2016).

[77] I. Lindgren, Phys. Rev. A **31**, 1273 (1985).

[78] G. Dixit, B. K. Sahoo, and R. K. Chaudhuri, and S. Majumder, Phys. Rev. A **76**, 042505 (2007); **76**, 059901(E) (2007).

[79] A. Bhowmik, N. N. Dutta, and S. Roy, Astrophys. J. **836**, 125 (2017).

[80] R. J. Bartlett and M. Musial, Rev. Mod. Phys. **79**, 291 (2007).

[81] A. Bhowmik, S. Roy, N. N. Dutta, and S. Majumder, J. Phys. B **50**, 125005 (2017).

[82] N. N. Dutta and S. Majumder, Phys. Rev. A **88**, 062507 (2013).

[83] N. N. Dutta and S. Majumder, Phys. Rev. A **85**, 032512 (2012).

[84] S. Biswas, A. Das, A. Bhowmik, and S. Majumder, Mon. Not. R. Astron. Soc. **477**, 5605 (2018).

[85] A. Kramida, Y. Ralchenko, J. Reader, and NIST ASD Team, 2016 NIST Atomic Spectra Database, version 5.4, http://physics.nist.gov/asd.

[86] S. A. Blundell, J. Sapirstein, and W. R. Johnson, Phys. Rev. D **45**, 1602 (1992).

[87] U. I. Safronova and M. S. Safronova, Phys. Rev. A **87**, 032501 (2013).

[88] W. R. Johnson, D. Kolb, and K.-N. Huang, At. Data Nucl. Data Tables **28**, 333 (1983).

[89] L. Visscher and K. G. Dyall, At. Data Nucl. Data Tables **67**, 207 (1997).

[90] F. A. Parpia, C. F. Fischer, and I. P. Grant, Comput. Phys. Commun. **175**, 745 (2006).

[91] U. I. Safronova, Phys. Rev. A **82**, 022504 (2010).

[92] U. I. Safronova, Phys. Rev. A **81**, 052506 (2010).

[93] N. N. Dutta, Hyperfine and parity non-conserving interactions in alkali-metal-like atoms and ions, Ph.D. dissertation, Indian Institute of Technology Kharagpur, 2014.

[94] B. Albrecht, Y. Meng, C. Clausen, A. Dareau, P. Schneeweiss, and A. Rauschenbeutel, Phys. Rev. A **94**, 061401(R) (2016).

[95] F. Schmidt, D. Mayer, M. Hohmann, T. Lausch, F. Kindermann, and A. Widera, Phys. Rev. A **93**, 022507 (2016).

[96] A. Fallon and C. Sackett, Atoms **4**, 12 (2016).